

1 Loss of Immiscible Nitrogen from Metallic Melt Explains Earth's Missing Nitrogen

2

3 *Jiachao Liu¹, Susannah Dorfman¹, Mingda Lv¹, Jie Li², Feng Zhu², Yoshio Kono^{3, 4}*

4 ¹*Department of Earth and Environmental Sciences, Michigan State University, MI 48824, USA*

5 ²*Department of Earth and Environmental Sciences, University of Michigan, MI 48109, USA*

6 ³*HPCAT, Geophysical Laboratory, Carnegie Institution of Washington, IL 60439, USA*

7 ⁴*Geodynamics Research Center, Ehime University, Ehime 790-8577, Japan*

8

9 **Nitrogen and carbon are essential elements for life, and their relative abundances in**
10 **planetary bodies are important for understanding planetary evolution and**
11 **habitability. The high C/N ratio in the bulk silicate Earth (BSE) relative to chondrites**
12 **has been difficult to explain through partitioning during core formation and**
13 **outgassing from molten silicate. Here we propose a new model that may have released**
14 **nitrogen from the metallic cores of accreting bodies during impacts with the early**
15 **Earth. Experimental observations of melting in the Fe-N-C system via synchrotron**
16 **X-ray radiography of samples in a Paris-Edinburgh press reveal that above the**
17 **liquidus, iron-rich liquid and nitrogen-rich fluid coexist at pressures up to at least 7**
18 **GPa. The combined effects of N-rich fluid lost to Earth's atmosphere and/or space as**
19 **well as N-depleted alloy equilibrating with the magma ocean on its way to the core**
20 **would help increase the BSE C/N ratio to match current estimates.**

21

22 **Introduction**

23 The habitability of Earth and other planetary bodies depends on the incorporation,
24 distribution, and speciation of volatile elements including carbon and nitrogen. In Earth,
25 the BSE C/N ratio is estimated to be higher than that of planetary building blocks
26 including enstatite and carbonaceous chondrites and interstellar dust and gas (e.g. Bergin
27 *et al.*, 2015; Marty, 2012). **Recent studies estimate the BSE C/N ratio to be**
28 **superchondritic based on measurements of gas bubbles trapped in mid-ocean ridge and**
29 **ocean island basalts (Bergin *et al.*, 2015; Halliday, 2013; Marty, 2012), and the estimated**

30 **BSE C/N ratio converges to 46 ± 9 recently (Bergin *et al.*, 2015).** In contrast, C/N ratios
31 measured in primitive CI chondrites (17 ± 3 , Alexander *et al.*, 2013) and enstatite
32 chondrites (14 ± 12 , Grady and Wright, 2003) are significantly lower. Explaining these
33 observations thus requires one or more mechanisms that preferentially deplete N relative
34 to C from the mantle source of basaltic magmas.

35 The key processes responsible for C and N redistribution among Earth reservoirs
36 were equilibrium partitioning the magma ocean and the growing metallic core, **plus**
37 degassing of the magma ocean to the early atmosphere, but these processes have been
38 insufficient to explain the **estimated** high BSE C/N ratio (Bergin *et al.*, 2015; Dalou *et al.*,
39 2017; Hirschmann, 2016). Core formation is expected to decrease the BSE C/N ratio
40 because at relevant conditions C is a much stronger siderophile element than N (Dalou *et al.*,
41 2017). Degassing has been thought to not significantly affect the C/N ratio, as
42 chemical analysis of volatiles in silicate glasses quenched from high pressure-temperature
43 (*P-T*) experiments indicates that the solubilities of C and N in the magma ocean are
44 comparable (Hirschmann, 2016).

45 The major host phase for both C and N in the solidifying planet is likely to be core-
46 forming alloy, therefore the Fe-N-C system under relevant conditions may hold the key to
47 the paradox of the high BSE C/N ratio. While the Fe-C phase diagram has been well
48 studied over a wide range of pressures (Fei and Brosh, 2014), very limited data are
49 available on the phase relations of the Fe-N system (Guillermet and Du, 1994). However,
50 melting behavior is expected to be different in these two systems with enrichment in the
51 light element, as the C-rich end member, graphite/diamond, has a melting point of 4000-
52 5000 K at relevant pressures (Grumbach and Martin, 1996), while the N-rich end member
53 would be gas/supercritical fluid in the BSE.

54

55 **Immiscible N-rich Fluid**

56 In order to test whether the mobility of N-rich gas/fluid could provide a possible
57 mechanism to leak N during accretion and core formation, we investigated melting
58 relations in the Fe-N-C system under high pressures by *in-situ* X-ray radiography and X-

59 ray diffraction (XRD) coupled with Paris-Edinburgh cells and *ex-situ* chemical analysis.
 60 The starting materials are either iron nitrides (Fe_3N and Fe_4N) or a mixture of iron and
 61 iron nitride powders with or without graphite powder with starting N and C contents
 62 ranging from 0-7.7 wt% and 0-10.0 wt.%, respectively (Table S-1). **A standard PE**
 63 **sample assembly configuration is employed (Kono *et al.*, 2014), which uses X-ray**
 64 **transparent MgO as the sample capsule and cylindrical graphite tube outside sample**
 65 **capsule as the heater.** Assemblages were first compressed to target pressures and
 66 gradually heated to fully melt the samples. Then the molten samples were quenched
 67 below 500 K within 5 seconds to preserve compositions for *ex-situ* chemical analysis
 68 (Table S-1).

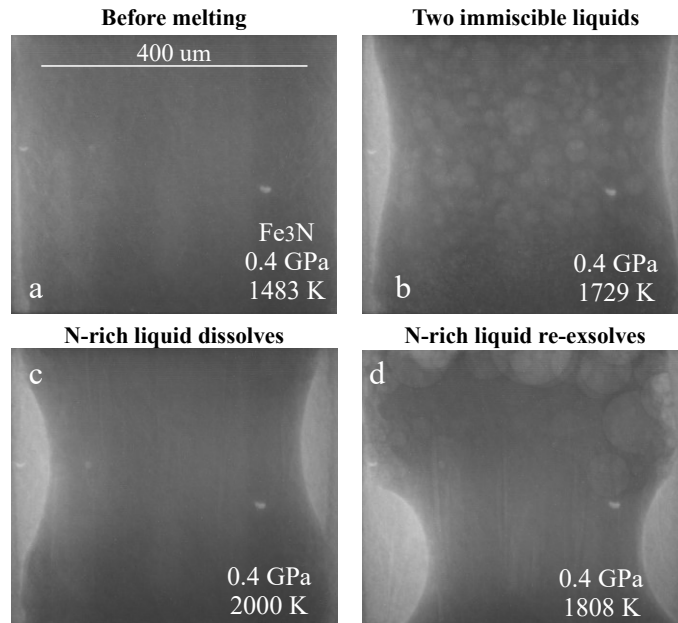


Figure 1 Representative X-ray radiographic images showing the evolution of miscibility gap in Fe-N-C system under high-pressure and high-temperature conditions (run 4-17). This *in-situ* X-ray radiography experiment starts at 0.4 GPa with Fe_3N as the starting material. **a**, The sample is below solidus at 0.4 GPa and 1483 K. **b**, Around 1729 K, immiscible N-rich supercritical fluid coexists with metallic liquid. **c**, At higher temperatures, N-rich supercritical fluid partially dissolves into metallic liquid. **d**, Lowering temperatures re-exsolves N-rich supercritical fluid from metallic liquid. The corresponding video is shown in Movie S-1.

70 Below the solidus, starting materials for all runs were homogenous at $\sim 3 \mu\text{m}$ spatial
71 resolution of X-ray radiographic images (e.g. Fig. 1a). An upper bound for the onset of
72 partial melting at higher temperature was indicated by the appearance of 10s-micron
73 regions of low X-ray absorption (e.g. Fig. 1b). At higher temperatures, these lighter
74 regions merge to form 10s to 100s-micron droplets which move vigorously (Fig. 1b).
75 XRD patterns during heating also recorded the melting process (Fig. S-1d): at 0.4 GPa
76 and 300 K, the XRD pattern confirmed Fe_3N as the starting material; at ~ 1690 K, most
77 crystalline peaks disappeared with obvious background lifting at $\sim 34\text{-}80$ keV (Fig. S-1d),
78 which originated from diffuse scattering. The corresponding X-ray radiographic image
79 (Fig. S1-b) showed the ubiquitous occurrence of the low X-ray absorption regions.
80 Therefore, both XRD and X-ray radiographic image indicated a partially molten state of
81 the Fe-N sample. Turbulent flow of two phases occurred above ~ 1725 K (Movie S-1),
82 and XRD patterns exhibited diffuse scattering with no XRD peaks (Fig. S-1d) and thus
83 indicated conditions above the liquidus but below a solvus. At higher temperatures, the
84 immiscible droplets partially dissolved into the metallic liquid but persisted to the highest
85 temperature investigated of run 4-17 (~ 2000 K, Fig. 1c). Lowering temperature makes
86 more immiscible droplets re-exsolved (Fig. 1d), confirming that the disappearance of the
87 immiscible droplets from Fig. 1b to 1c cannot be explained by loss through the MgO
88 capsule. In comparison, no inhomogeneity appeared at all in Fe melting experiment at 0.8
89 GPa up to 2103 K (Fig. S-2).

90 The immiscible droplets with lighter colors in X-ray radiographic images are enriched
91 in N because the contrast in X-ray radiographic images reflects density difference (Kono
92 *et al.*, 2015). The N-rich nature of the immiscible fluid is confirmed by *ex-situ* chemical
93 analysis of the quenched samples: for experiments quenched with the presence of
94 immiscible liquids, the regions which are lighter in X-ray radiographic images
95 correspond to voids in recovered samples (e.g. Fig. S-3, S-5 and S-6); N contents in the
96 recovered samples are lower than the starting values when immiscible melting occurs
97 (Table S-1). For example, N content in run 4-16 decreases from 5.9% in the starting
98 materials to 1.5% in the recovered sample (Fig. S-3). With increasing temperature, the
99 increase of N solubility in metallic melt (e.g. Fig. 1 and Movie S-1) can be explained by
100 the concave-down shape of the solvus, which marks the phase boundary between one

101 miscible liquid and two immiscible liquids (Fig. S-4). Similar phenomenon has been
 102 observed in Fe-O system (Kowalski and Spencer, 1995; Tsuno *et al.*, 2007): at 1 bar, O
 103 solubility increases from ~0 to ~5 mol.% when temperature increases from ~1811 K to
 104 ~2340 K (Kowalski and Spencer, 1995). Such a miscibility gap persists to at least 21 GPa
 105 in Fe-O system and O solubility in metallic melt increases with a rate of 0.01-0.03 mol./K
 106 between 15-21 GPa and 2050-2350 K (Tsuno *et al.*, 2007). For experiments with C added
 107 to the starting materials, immiscible melting still occurs (Fig. S-5 and S-6). C contents in
 108 the recovered samples are the same as starting materials within uncertainty (Table S-1).
 109 This indicates that C did not dissolve into N-rich fluid during immiscible melting.
 110

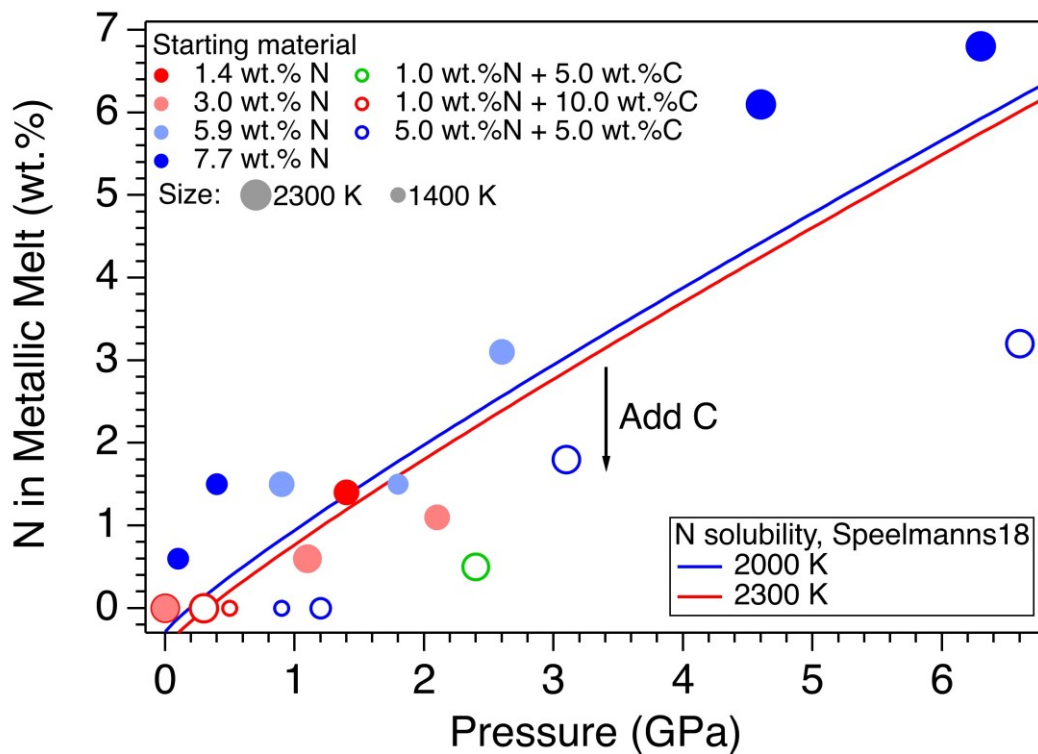


Figure 2 The pressure dependence of N solubility in Fe-N-C melt. The circles are from our experiments: the solid ones are for Fe-N starting materials; the open ones are for Fe-N-C starting materials. Symbol size is proportional to the temperature (1400-2300 K) at which the experiments were quenched and color indicates initial composition (see legend). The blue and red curves are modeled N solubility in Fe-N-C melt at 2000 K and 2300 K, respectively, from Speelmanns *et al.* (2018).

111

112 The combination of *in-situ* and *ex-situ* analysis was employed to constrain the
 113 solubility of N in Fe-N-C alloys (Fig. 2). Near 1 bar in all compositions up to 7.7 wt% N

114 and 10.0 wt.% C, immiscibility of N-rich supercritical fluid and metallic melt observed
115 *in-situ* persists to 2273 K, the highest temperature investigated here. Solubility of N in
116 Fe-N-C alloy increases from almost 0 near 1-bar conditions to ~6.8 wt.% N at 6.3 GPa, as
117 the highest pressure investigated here (Fig. 2). And the pressure required for closing the
118 miscibility gap increases with the starting N and C contents (Fig. 2). For Fe-1.4 wt.%N
119 starting material at about 0-0.1 GPa, immiscible liquids persist to at least 1980 K, but no
120 immiscible liquids appear at ~1.4 GPa up to 2000 K (Fig. S-7). In contrast, for Fe-7.7
121 wt.% N starting composition the solvus persists to at least 6.3 GPa (Fig. 2). Adding 5-10
122 wt% C in the starting materials expands the pressure range of the solvus by about 2-5
123 GPa (Fig. 2). This is because C is more siderophilic than N and it expels N from metallic
124 melt to the immiscible fluid.

125 A recent study also infers the presence of N-rich fluid from Fe-N-C melt based on the
126 *ex-situ* analysis of quenched samples (Speelmanns *et al.*, 2018). The trend of their N
127 solubility model is consistent with our data as it increases with pressure (Fig. S-8).
128 However, due to C and Pt contaminations from sample capsules (Speelmanns *et al.*,
129 2018), the effect of C on N solubility is not incorporated in their model. The presence of
130 5.0 wt.% C lowers N solubility by 1-3 wt.% (Fig. S-8), therefore C and other more
131 siderophilic elements (e.g. sulfur) significantly lower N solubility in metallic liquid at
132 high pressures (e.g. Dalou *et al.*, 2017). The presence of immiscible N-rich fluid in
133 silicate-alloy system has been observed in a previous partitioning study on metallic-
134 silicate melts up to 10 GPa (Roskosz *et al.*, 2013), supporting that this immiscible
135 phenomenon could occur in a realistic magma ocean phase assemblage.

136

137 **Missing N in the Mantle**

138 The conundrum of missing N in the mantle can be solved by accounting for
139 immiscibility of N in the Fe-N-C system in modeling Earth's N budget. Our model
140 calculates the BSE C/N ratio in three steps (Fig. S-9 and SI): First, we assume Earth-
141 forming impactors have alloy core and silicate mantle in equilibrium with average
142 alloy/silicate mass ratio of 0.46, same as the Earth's core/mantle mass ratio. The amount
143 of N stored in metallic core is controlled by oxygen fugacity (Dalou *et al.*, 2017): 90.2%
144 N would stay in the core at oxidized bodies (ΔIW -0.5 to -1.0); this number decreases to

145 69.7% and 12.1% at modestly reduced (ΔIW -1.8 to -2.2) and more reduced bodies (ΔIW -
146 3.4 to -3.6), respectively (Fig. S-10). **In contrast, previous models assume all C and N**
147 **were initially stored in silicate (Bergin *et al.*, 2015; Dalou *et al.*, 2017; Hirschmann,**
148 **2016). This assumption sets the initial BSE C/N ratio at 25 without loss of the primordial**
149 **atmosphere, which is about 20-24 higher than our initial BSE C/N ratios (Fig. 3).**

150 Secondly, we assume that extensive melting of alloy during high-energy impacts induces
151 immiscible melting, resulting in loss of all N stored in impactor cores to space. In
152 general, the fraction of N released from an impactor depends on the core/mantle mass
153 ratios in the accreting bodies; the degree of melting during accretion/melting; the extent
154 of immiscibility between N-rich supercritical fluid and metallic melt, and the fraction of
155 atmospheric N loss to space. As our model assumes impactor cores melt completely and
156 release N at the magma ocean surface, it yields an upper limit for N loss at this stage. The
157 loss of N results in extremely large C/N ratio in the metallic phase. Once such N-depleted
158 metallic droplets sink below the depth where solubility of N in alloy increases (Fig. S-9),
159 N could partition from the magma ocean into N-depleted alloy droplets and therefore
160 elevate the BSE C/N ratio as the alloy joins Earth's growing core.

161 Overall, the loss of N from impactor cores could significantly lower Earth's bulk N
162 budget and therefore raise the BSE C/N ratio (Fig. 3). Because N partitions more strongly
163 into alloy under more oxidized conditions, more N is subject to loss from oxidized
164 accreting bodies (Fig. S-10). Similarly, the subsequent core formation would also result
165 in higher C/N ratio of the BSE under oxidized conditions. Over time during core
166 formation, f_{O_2} is estimated to evolve from lower values of ΔIW -3.9 to ΔIW -1.9 to higher
167 values of ΔIW -1.9 to ΔIW -1.0 (Rubie *et al.*, 2011, Badro *et al.*, 2015). Therefore, the
168 BSE C/N ratio is expected to evolve from 0.03-0.5 at very reduced conditions to 0.7-41.4
169 at reduced conditions and finally to 5-130.0 at slightly reduced conditions (Fig. 3).

170 Compared with previous models (Bergin *et al.*, 2015), our model matches the estimated
171 BSE C/N ratio for an extensive range of redox conditions, the degree of alloy-silicate re-
172 equilibration and extent of loss of nascent atmosphere during accretion and core
173 formation. **Notably, both C and N form accessory minerals, such as diamonds, iron**
174 **carbides, iron/titanium/chromium nitrides (e.g. Fegley, 1983; Javoy, 1997; Kaminsky and**
175 **Wirth, 2017), which has not been considered in the estimated BSE C/N ratio yet. In**

176 addition, the presence of deep-mantle carbonates (e.g. Brenker *et al.*, 2007) and high
177 solubilities (10s to 1000s $\mu\text{g/g}$) of N in transition zone and lower mantle minerals
178 (Yoshioka *et al.*, 2018), both of which are sensitive to redox and pH conditions (e.g.
179 Mikhail *et al.*, 2017; Rohrbach and Schmidt, 2011), would also influence the estimation
180 of the BSE C/N ratio.

181

182 Vaporization during accretion has recently been evoked to explain Mg, Si and Fe
183 isotopic compositions in the BSE (Hin *et al.*, 2017) and the pattern of volatile element
184 depletion (Norris and Wood, 2017), indicating its critical role in the early stage of Earth
185 evolution. Considering the high C/N ratios (>10) of most planetary bodies (Bergin *et al.*,
186 2015), the C/N ratios of the impactors' cores would be even higher and therefore promote
187 immiscible melting during impact. In addition, the loss of N through immiscible fluid
188 could be even more significant for Earth-like planets at a synestia stage (Lock and
189 Stewart, 2017): in this stage, the magma ocean is surrounded by massive vaporized
190 materials, which are at pressures between 0.1 bar and 1.0 GPa.

191

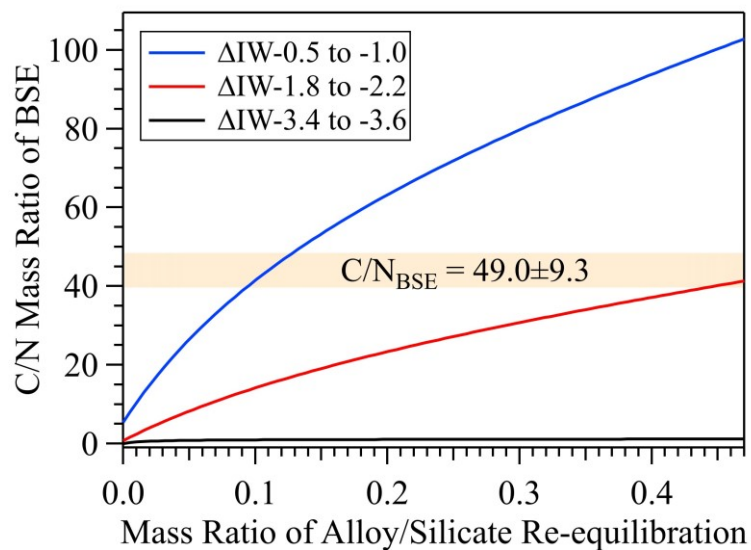


Figure 3 The evolution of the BSE C/N ratio with the degree of re-equilibration between alloy and silicate during core formation. The blue curve is calculated at reduced conditions ($\Delta\text{IW}-0.5$ to $\Delta\text{IW}-1.0$); the red curve is for reduced conditions

(ΔIW -1.8 to ΔIW -2.2) and the black curve is for very reduced conditions (ΔIW -3.4 to ΔIW -3.6). The horizontal yellow bar marks the range of the **estimated** present BSE C/N ratio (Bergin *et al.*, 2015).

192

193 **References**

194 Alexander, C.M.O., Howard, K.T., Bowden, R., Fogel, M.L. (2013) The classification of
195 CM and CR chondrites using bulk H, C and N abundances and isotopic
196 compositions. *Geochimica et Cosmochimica Acta* 123, 244–260.

197 Badro, J., Brodholt, J.P., Piet, H., Siebert, J., Ryerson, F.J. (2015) Core formation and
198 core composition from coupled geochemical and geophysical constraints.
199 *Proceedings of the National Academy of Sciences* 112, 12310–12314.

200 Bergin, E.A., Blake, G.A., Ciesla, F., Hirschmann, M.M., Li, J. (2015) Tracing the
201 ingredients for a habitable earth from interstellar space through planet formation.
202 *Proceedings of the National Academy of Sciences* 112, 8965–8970.

203 Brenker, F.E. *et al.* (2007) Carbonates from the lower part of transition zone or even the
204 lower mantle. *Earth and Planetary Science Letters* 260, 1–9.

205 Dalou, C., Hirschmann, M.M., von der Handt, A., Mosenfelder, J., Armstrong, L.S.
206 (2017) Nitrogen and carbon fractionation during core–mantle differentiation at
207 shallow depth. *Earth and Planetary Science Letters* 458, 141–151.

208 Fegley, B. (1983) Primordial retention of nitrogen by terrestrial planets and meteorites.
209 *Journal of Geophysical Research: Solid Earth* 88, A853–A868.

210 Fei, Y., Brosh, E. (2014) Experimental study and thermodynamic calculations of phase
211 relations in the Fe–C system at high pressure. *Earth and Planetary Science*
212 *Letters* 408, 155–162.

213 Grady, M.M., Wright, I.P. (2003) Elemental and Isotopic Abundances of Carbon and
214 Nitrogen in Meteorites. *Space Science Reviews* 106, 231–248.

215 Grumbach, M.P., Martin, R.M. (1996) Phase diagram of carbon at high pressures and
216 temperatures. *Physical Review B* 54, 15730–15741.

217 Halliday, A.N. (2013) The origins of volatiles in the terrestrial planets. *Geochimica et*
218 *Cosmochimica Acta* 105, 146–171.

219 Hin, R.C. *et al.* (2017) Magnesium isotope evidence that accretional vapour loss shapes
220 planetary compositions. *Nature* 549, 511–515.

- 221 Hirschmann, M.M. (2016) Constraints on the early delivery and fractionation of Earth's
 222 major volatiles from C/H, C/N, and C/S ratios. *American Mineralogist* 101, 540–
 223 553.
- 224 Javoy, M. (1997) The major volatile elements of the Earth: Their origin, behavior, and
 225 fate. *Geophysical Research Letters* 24, 177–180.
- 226 Kaminsky, F., Wirth, R. (2017) Nitrides and carbonitrides from the lowermost mantle
 227 and their importance in the search for Earth's "lost" nitrogen. *American*
 228 *Mineralogist* 102, 1667–1676.
- 229 Kono, Y., Kenney-Benson, C., Shibazaki, Y., Park, C., Wang, Y., Shen, G. (2015) X-ray
 230 imaging for studying behavior of liquids at high pressures and high temperatures
 231 using Paris-Edinburgh press. *Review of Scientific Instruments* 86, 072207.
- 232 Kono, Y., Park, C., Kenney-Benson, C., Shen, G., Wang, Y. (2014) Toward
 233 comprehensive studies of liquids at high pressures and high temperatures:
 234 Combined structure, elastic wave velocity, and viscosity measurements in the
 235 Paris–Edinburgh cell. *Physics of the Earth and Planetary Interiors* 228, 269–280.
- 236 Kowalski, M., Spencer, P.J. (1995) Thermodynamic reevaluation of the C-O, Fe-O and
 237 Ni-O systems: Remodelling of the liquid, BCC and FCC phases. *Calphad* 19,
 238 229–243.
- 239 Lock, S.J., Stewart, S.T. (2017) The structure of terrestrial bodies: Impact heating,
 240 corotation limits, and synestias. *Journal of Geophysical Research: Planets* 122,
 241 2016JE005239.
- 242 Marty, B. (2012) The origins and concentrations of water, carbon, nitrogen and noble
 243 gases on Earth. *Earth and Planetary Science Letters* 313–314, 56–66.
- 244 Mikhail, S., Barry, P.H., Sverjensky, D.A. (2017) The relationship between mantle pH
 245 and the deep nitrogen cycle. *Geochimica et Cosmochimica Acta* 209, 149–160.
- 246 Norris, C.A., Wood, B.J. (2017) Earth's volatile contents established by melting and
 247 vaporization. *Nature* 549, 507–510.
- 248 Rohrbach, A., Schmidt, M.W. (2011) Redox freezing and melting in the Earth's deep
 249 mantle resulting from carbon-iron redox coupling. *Nature* 472, 209–212.
- 250 Roskosz, M., Bouhifd, M.A., Jephcoat, A.P., Marty, B., Mysen, B.O. (2013) Nitrogen
 251 solubility in molten metal and silicate at high pressure and temperature.
 252 *Geochimica et Cosmochimica Acta* 121, 15–28.
- 253 Rubie, D.C., Frost, D.J., Mann, U., Asahara, Y., Nimmo, F., Tsuno, K., Kegler, P.,
 254 Holzheid, A., Palme, H. (2011) Heterogeneous accretion, composition and core–
 255 mantle differentiation of the Earth. *Earth and Planetary Science Letters* 301, 31–
 256 42.

- 257 Speelmanns, I.M., Schmidt, M.W., Liebske, C. (2018) Nitrogen Solubility in Core
258 Materials. *Geophysical Research Letters* 45, 7434–7443.
- 259 Tsuno, K., Ohtani, E., Terasaki, H. (2007) Immiscible two-liquid regions in the Fe–O–S
260 system at high pressure: Implications for planetary cores. *Physics of the Earth and*
261 *Planetary Interiors* 160, 75–85.
- 262 Yoshioka, T., Wiedenbeck, M., Shcheka, S., Keppler, H. (2018) Nitrogen solubility in the
263 deep mantle and the origin of Earth’s primordial nitrogen budget. *Earth and*
264 *Planetary Science Letters* 488, 134–143.
- 265